NJC

Accepted Manuscript

This is an *Accepted Manuscript*, which has been through the Royal Society of Chemistry peer review process and has been accepted for publication.

Accepted Manuscripts are published online shortly after acceptance, before technical editing, formatting and proof reading. Using this free service, authors can make their results available to the community, in citable form, before we publish the edited article. We will replace this *Accepted Manuscript* with the edited and formatted *Advance Article* as soon as it is available.

You can find more information about *Accepted Manuscripts* in the Information for Authors.

Please note that technical editing may introduce minor changes to the text and/or graphics, which may alter content. The journal's standard Terms & Conditions and the Ethical guidelines still apply. In no event shall the Royal Society of Chemistry be held responsible for any errors or omissions in this *Accepted Manuscript* or any consequences arising from the use of any information it contains.

ROYAL SOCIETY OF CHEMISTRY

www.rsc.org/njc

New Journal of Chemistry

ARTICLE

Lamellar-Structured Biomass-Derived Phosphorus- and Nitrogen-co-Doped Porous Carbon for High Performance Supercapacitors

Received 00th January 20xx,
Accepted 00th January 20xx

DOI: 10.1039/x0xx00000x

www.rsc.org/

Jie Wang,[a] Laifa Shen,[a] Yunling Xu,[a] Hui Dou[a] and Xiaogang Zhang*[a]

As electrical energy storage and delivery devices, carbon-based supercapcitors have attracted much attention for advancing the energy-efficient economy.It is important to develop facile, low-cost and environmentally friendly method to produce novel carbon materials. In this study, we report a scalable synthesis of phosphorus- and nitrogen-co-doped porous carbons using lamellar-structured fish scale. The special lamellar structure of fish scale allow to produce porous carbons with high specific surface areas (up to 1300 $m^2 g^{-1}$) and high level of mesoposity. The inherent organic composition could be oriented to abundant N and P functional groups on the final carbons. The high levels of porosity and rich surface functionality permit the carbons to show excellent electrochemical performance as electrode materials for supercapacitors. The energy densities of supercapacitors approach 11.7 and 33.1Wh kg^{-1} in aqueous and IL electrolyte, respectively.

Introduction

The rising environmental concerns together with development of energy-efficient economy have created an ever-increasing demand for energy-storage devices for clean energy, such as wind and solar energy. Among the available energy-storage devices, supercapacitors are the most efficient high-power applications. They are able tostore and release energy within a very short period, being perfectly adapted for the quality of electricity required by energy efficient industrial equipment, electric and hybrid electric vehicles and smart-grid applications. Based on the charge-storage mechanism, supercapacitors are categorized as either electrical double-layer capacitors (EDLCs) or pseudocapacitors. The capacitance of EDLCs comes from the pure electrostatic charge accumulated at the electrode/ electrolyte interface. It requires electrode materials with high surface area and suitable pores adapted to the size of ions.[1] Nanoporous carbons with large specific surface area (SSA) and good electrical conductivity, such as activated carbon, carbon nanotubes, graphene, and hierarchically porous carbon have been widely used as electrode materials for EDLCs.[2-6] Alternatively, pseudocapacitors developed from the surface redox process exhibit higher charge densities but suffer from slower charge transfer kinetics compared to EDLCs.[1, 7, 8]Hence, one of the most critical aspects in the development of supercapacitor technologies is to provide higher energy and power delivery, while maintaining excellent cycle stability.

To meet such a demand, porouscarbon materials with developed porous structure combining favorable electronic structure and active surface chemistry (heteroatom-doping) is expected to show superior ability as supercapacitor electrodes.[9, 10] Several efforts have been devoted to modify the surface of carbon materials by doping with heteroatoms (N,[11-14]B,[15-17] P,[18]S[14, 19]). These heteroatoms doping not only improves the wettablility of carbon materials but also gives an acid-base character, enhancing their capacitance by the pseudo-capacitive effect. The N-doping can modulate the inherent electrical properties of carbon, favoring for the enhanced power property;[11, 13] P atoms can stabilize oxygen functional groups during electrochemical charging, thereby improving the reaction stability.[18] In general, two strategies are applied to incorporate the heteroatoms into the porous carbon materials. One is post-treatment of carbonaceous matrix with ammonia, H_3BO_3 or H_3PO_4 at a high temperature to introduce functional groups on their surfaces.[14, 15, 18] However, considering the different intrinsic properties of inorganic acids and organic framework, the doped heteroatoms are rather heterogeneous in distribution.[20] The other is *in situ* doping by employing petrochemically derived materials such as polypyrrole,[21, 22] polyaniline,[23, 24]polyacrylonitrile,[25] to make a more homogeneous incorporation of the N species into the carbons with controlled chemistry. However, the multi-step synthesis procedure of polymers shows uncompetitive price-to-performance ratio and inevitably restricts their commercial viability.

Alternatively, direct carbonization of low-cost biomass emerges as a cost-effective strategy to yield heteroatom-doped carbon materials with high energy and power densities.[26-30] In our lives, there are millions-tons of biomasses

[a] Jiangsu Key Laboratory of Materials and Technology for Energy Conversion, College of Material Science and Engineering, Nanjing University of Aeronautics and Astronautics, Nanjing, 210016, P. R. China.

† Electronic Supplementary Information (ESI) available: [SEM, TEM, PSD, XRD and Raman of SAC, and electrochemical measurement]. See DOI: 10.1039/x0xx00000x

wastes containing a rich nutritional and chemical composition available per day. For example, by direct carbonization of silk, novel heteroatom containing carbon nanoplates are prepared and capacitance of 264F g^{-1} is achieved.[31] The porous carbon obtained by chemical activation of chicken eggshell membranes shows a capacitance of 297 F g^{-1}in 1 M H_2SO_4 and 284 F g^{-1} in 6 M KOH.[32] In addition, seaweeds,[33] egg white,[27] human hair,[34] watermelon,[35] cornstalk[36] and many other biomass have also been used to prepare carbon materials. Fish scale is one of the most abundant biomass wastes all over the world. The main fraction of scale are abundant protein and plenty lecithin, which contain abundant N and P functional groups. In addition, the presence of trace amount of some inorganic component (typically Fe, Zn and Ca) could promote the graphitization relatively during carbonization. Furthermore, unlike other biomass, fish scale is composed of lamellar structure.[37, 38] In this study, we report a combined pre-carbonization and chemical activation processes by using fish scale as the precursor to achieveP- and N-co-doped porous carbons (SAC). The unique feature of fish scale enables formation of laminar shaped carbon and high levels of porosity, providing a favorable path for transportation and penetration of electrolyte ions. The abundant functional groups ideally suited electrochemical energy storage. As expected the SAC display remarkable electrochemical properties in both aqueous and ionic liquid electrolyte.

2. Experimental

2.1. Materials Synthesis

The scale-derived activated carbon (SAC) materials were prepared through a two-step method. Typically, the fish scale derived from crucian carp was washed by water and ethanol and freezedried for 24 h. The dried fish scale was carbonized in a tubular furnace with an N_2 flow at 700 °C for 2 h. Then, the pre-carbonized product was mixed with KOH pellets in an agate mortar. The resulted mixture was transferred into the tubular furnace and then heated to 600 °C under N_2 flow for 1 h at a heating rate of 5 °C min^{-1}. Then, the obtained sample, denoted as SAC-X (Xrefers to the mass ratio of pre-carbonized product to KOH), was washed in 2 M HCl and distilled water to remove any metal residuals. For comparison, scale derived carbon without activation is referred as SC.

2.2. Material Characterization

The structure and morphology of prepared productswere characterized by X-ray diffraction measurement (XRD, Bruker-AXS D8 DISCOVER using Cu Kα radiation),Raman-laser spectrometer (Jobin-Yvon Labram HR800), scanning electron microscopy (SEM,JEOL JSM-6380LV FE-SEM) and transmission electron microscopy (TEM, FEI, Tecnai-20), respectively. The X-ray photoelectron spectroscopy (XPS) analysis was performed on a Perkin-Elmer PHI 550 spectrometer with Al Kα (1486.6 eV) as the X-ray source.The nitrogen (N_2) adsorption-desorption isotherms of the samples were conducted by using a Micromeritics BK122T-B analyzer. Pore size distribution (PSD)pore volumeis obtained using data evaluation by the Barrett-Joyner-Halenda(BJH) method.

2.3 ElectrochemicalMeasurements

All the electrochemical measurements were carried out on a CHI 660D electrochemical workstation system. Fist, the supercapacitive performance tests were performed in a conventional three-electrode system with 6 M KOH as the electrolyte. Platinum foil and a saturated calomel electrode (SCE) were used as counter and reference electrodes, respectively. The working electrodes were prepared by mixing active material (5 mg), acetylene black and polytetrafluorene-ethylene (PTFE) binder with a weight ratio of 80:10:10. After coating the above slurries on foamed Ni grids (1×1 cm^2), the electrodes were dried at 60 °C for several hours before pressing under a pressure of 15 MPa. Two-electrode system tests were conducted in a 2016-type cell with two nearly identical (by weight and size) film electrodes using glass fiber (GF/D, Whatman) as separator. The assembly process was carried out in an argon-filled glove box. The working electrode was fabricated by mixing SAC-1 (80 wt%), acetylene black(10 wt%) and PTFE (10 wt%) in ethanol to forma slurry. The mixture was blended completely, rolled into a thin film and punched into circular sheets. Then, the circular sheets were hot pressed onto current collectors. 1-ethyl-3-methylimidazolium tetrafluoroborate (EMImBF_4, >98%) was used as electrolyte for two-electrode system. Thecapacitances *C* can be calculated from the galvanostatic charge/discharge (GCD) curves according to the equation:

$$C = \frac{I\Delta t}{m\Delta V}$$

where *I*, *t*, *m* and *V* is the current density, discharge time, mass of the active material and the voltage change, respectively.
The capacitance for a single electrode C_{single}(F g^{-1}) can be calculated by evaluating the GCD curves according to equation:

$$C_{single} = \frac{4I\Delta t}{m\Delta V}$$

where *I* refers to the applied current density, *t*represents the discharge time, *m* is the total mass of the active material on the two electrodes, and *V* corresponds to the voltage change. The energy density (*E*) of a supercapacitor depends on its specific capacitance (*C*) and operating voltage (*V*):

$$E = \frac{1}{2}CV^2$$

3. Results and discussion

3.1 Preparationand characterization of SAC

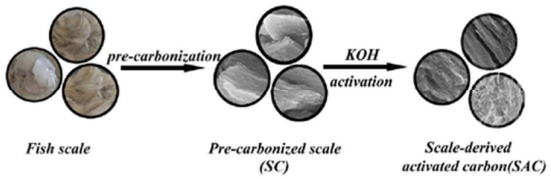

Fig. 1 Schematic illustration of the preparation of SAC.

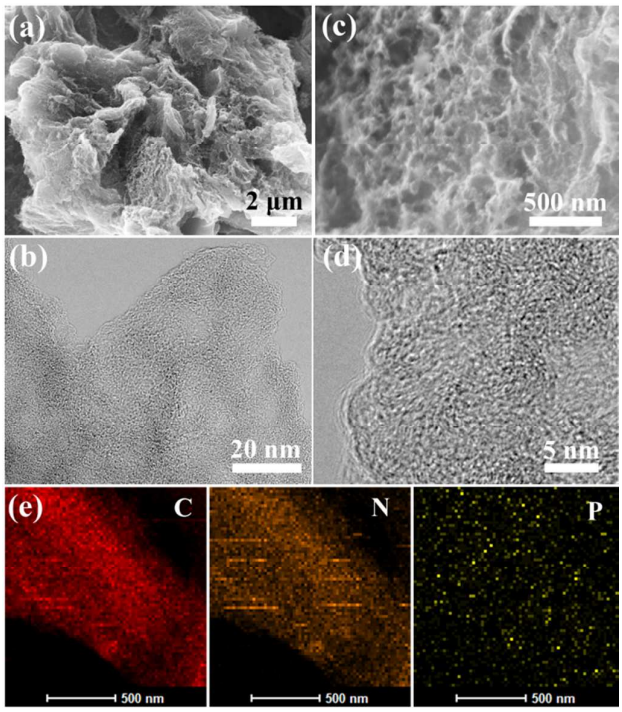

Fig. 2(a, b)SEM images, (c, d)TEM images, and (e) corresponding elemental mapping of activated carbon SAC-1.

A schematic illustration for the preparation procedure of SAC is presented inFig. 1. To allow for the uniform pore broadening and achieve optimum PSD and higher SSA, the fish scale is first pre-carbonized before activation. In this work, we aim to investigate the influence of the amount of KOH on the SSA and heteroatoms doping. Therefore, the pre-treated chars are then grounded with KOH and further activated at 600 °C. During the activation process, KOH melts and penetrates into the connection between the chars, further generating micro and mesoporosity. Fig.S1 displays the microstructure of the fish scale-derived carbon, highlighting that the lamellar structure is retained during the carbonization process. After chemical activation, the sheet-like microstructure is partially destroyed and a sponge-like microstructure constituted by 3D interconnected carbon walls is formed (Fig.2a and b). TEM (Fig. S2) images show that SAC still remain the lamellar structure with thin and connected carbon sheet. As observed from the high-resolutionTEM (HRTEM) images (Fig. 1c and d) of SAC, we could clearly see the continuous porous structure and interconnected worm-like nanopores. The lattice fringe spacing is about 0.34 nm, which corresponds to the graphite (002) plane, implying a high degree of graphitization. The good pore connectivity, which originated from the lamellar structure of SC, can prevent particle aggregation or layer-to-layer stacking during chemical activation. The elemental mapping images (Fig.2e) reveal the nature of doping in the SAC. Homogeneous N and P doping in a porous carbon matrix was achieved and the difference in the density of these spots in the samples indicates different concentration of atoms in the structure of the SAC-1 sample.

The structure of SAC was further studied by X-ray diffraction (XRD) and Raman spectroscopy. As observed in Fig.S3a, two typical broadened diffraction peaks appear at 2θ=24° and 43°, indicating the amorphous state of SAC. The Raman spectra clearly indicate the D-band peak at 1320 cm^{-1} and G-band at 1590 cm^{-1}(Fig.S3b). The G-band is attributed to the vibration of sp^2-bonded carbon atoms in a 2D hexagonallattice (E_{2g}mode), and the band is correlated to the (002) diffraction peak in the XRD pattern. The D-band is ascribed to the defect sites or disordered sp^2-hybridized carbon atoms of graphite. The intensity ratio of the G-band to the D-band (I_G/I_D) reveals the amount of structurally ordered graphite crystallites in the carbonaceous materials and is proportional to their crystallinity.[39, 40] The I_G/I_D value of the porous SAC-1 was calculated to be 1.03, which should be responsible for its good electronic conductivity.

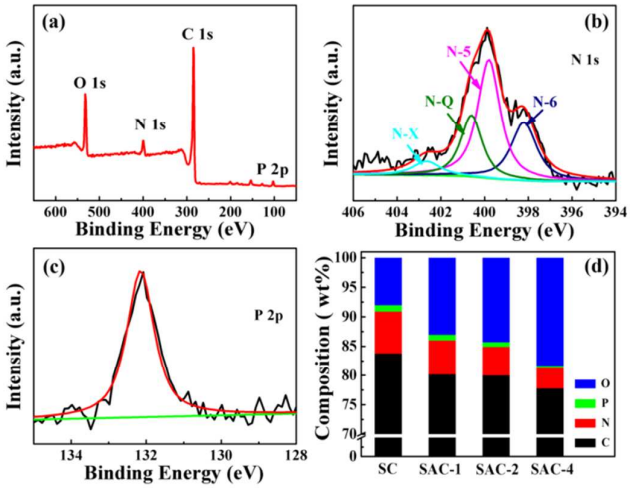

Fig. 3 XPS results for SAC-1: (a) survey scan, (b) N 1s, (c) P 2p, and (d) differentelement content in different samples.

The main components of fish scale are mineral salts, protein and phospholipid, with approximately 8-10 % N and 2-3 % P in its organic matter.[37]The N and P contents in pre-carbonized SC are estimated to be 6.88 % and 1.12 % by XPS analysis. After chemical activation, the XPS spectra (Fig. 3b) of SAC-1 show that the SAC-1 still consists of N and P, but the contents decrease to 5.74%and 0.98%, respectively. For SAC-1, the high-resolution N 1s core level XPS spectra can be deconvoluted into 4 peaks (Fig.3c), representing pyridinic N (N-6 at 398.0 ±0.2 eV), pyrrolic or pyridonic N (N-5 at 399.7 ±0.2 eV), quaternary N (N-Q at 400.8 ±0.2 eV) and oxidized N (N-X at 402.5 ±0.2 eV).[41]For P (Fig.3d), the binding energy around 133.0 eV can be assigned to C-O-PO_3 and/or C-PO_3 groups.[18, 42] The P bonded to N is reflected in the peaks at 398 eV and 401 eV that correspond to P=N and P–N bonds, respectively. The incorporation of P can form a protective layer at the surface and inhibit the formation of unstable surface oxygen groups. As shown in Fig. 3d and Table S1, with the increasing amount of KOH, the contents of the heteroatoms (N and P) gradually decrease. When compared with SC, however, the SAC samples contain more electro-active N functionalities, locating at the

edge of graphite plane (N-5, N-6, and N-X), and less N-Q functionalities that in the middle of graphite plane (N-Q) (Table S1). It is indicated although KOH activation has slightly reduce N content, it creates more N functional groups which are more beneficial to supercapacitive performance.[43]

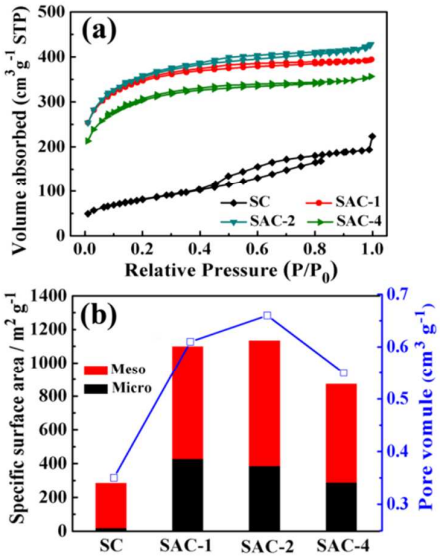

Fig. 4. (a) N_2 adsorption-desorption isotherms, (b) pore volume and SSA of micropore and mesopore of SC and SAC materials.

It is known that chemical activation will generate micro/mesopores inside carbons, with the surface area and porosity being controlled by the activation ratios. The N_2 sorption isothermal analysis in Fig. 3a demonstrates SAC and SC samples all exhibit type IV isotherms. But the broadening of the knee in the relatively low-pressure range for SAC suggests small mesopore developing with increased activation ratios. Fig. 4b summarizes the pore volume and SSA of different SC and SAC samples. It can be seen that both of SSA and pore volume first increase with activation ratio and then decreases. The SSA goes from 1098.5 m^2g^{-1} for SAC-1 to 1134.2 $m^2g^{-1}$for SAC-2, and then decreases to 871.7 m^2g^{-1} for SAC-4. The pore volume goes from 0.61 $m^3g^{-1}$for SAC-1 to 0.66 m^3g^{-1} for SAC-2, and then decreases to 0.55 m^2g^{-1} for SAC-4. It means that there is a critical amount of KOH after which the structure of the carbon materials just collapses, presumably due to severe reaction.[31, 34] It is worth noted that the SAC materials also show high mesopore ratio (SSA_{meso}/SSA calculated from Fig. 4b). For SAC-1, the mesopore ratio is up to 61%. The high level of mesoporosity could be mainly attributed to the lamellar structure of SC, which is beneficial to the diffusion and crystallization of KOH in the interior ofcarbon, rather than on the surface. The PSD curves of all the samples are shown in Fig.S4 and it is indicated that SAC carbons have the highest pore volume between 2 and 3 nm. The above characterizations demonstrate the unique features of SAC such as large SSA and high mesoporosity, hierarchical porous nanostructure and high-level heteroatom-doping. It is expected that they will have impressive electrochemical performance as electrode materials for supercapacitors. Compared to the previously reported template methods for porous carbons with hierarchical structure,[22, 44, 45] the present approach is much cheaper and easier for scalable preparation. Additionally, for the obtained hierarchical porous carbon, the SSA, pore volume, heteroatoms and their contents can be readily adjusted by changing the activating conditions.

3.2 Electrochemical performances

The electrochemical performance of SAC samples was first evaluated in a three-electrode system in 6 M KOH electrolyte. CV curvesof SC and SAC electrodes at different potential sweep ratesare compared in Fig. 5a and Fig.S5.All the curves show quasi-rectangular shape with a few humps, indicating that the synegistic effects of electric double-layer capacitance (EDLC) and pseudocapacitance related to the heteroatom functionalities. In addition, the remarkable difference in electrochemical surface activity between these samples can be easily recognized. In detail, the SC sample exhibits much smaller rectangular curves corresponding to its low capacitance, while the SAC-1 presents the largest capacitance. We also observe that the SAC-1 still kept the "rectangular shape" CV even at a potential scan rate of 500 mV s^{-1} (Fig. 5a), indicating a good capacitor response and low ESR. As shown in the galvanostatic charge/discharge (GCD) curves (Fig. 5b and Fig.S6), the discharging time of the SAC-1 is significantly longer compared with that of other materials at both high and low current densities, indicating that the SAC-1 offers a much larger capacitance, which agrees well with the results of CV tests. The GCD curves of SAC-1 exhibit a quasi-symmetric capacitive behavior. The small deviation from linearity demonstrates a pseudocapacitive contribution. At a current density of 1.0 A g^{-1}, the specific capacitance for the SAC-1 electrode is up to332 F g^{-1}, which ismore than twice that of the SC electrode (114 F g^{-1}) and is also much higher in comparison with the SAC-2 and SAC-4 (310 and 234 F g^{-1}, respectively). The greatly improved capacitance of SAC-1, especially compared with SC, is due to the substantially increased SSA for formation of electric double layer segregation.[46] As SAC-1 material possesses relatively smaller SSA than SAC-2, this result suggests that the higher content of N and P in the carbon matrix is responsible for an important capacitive contribution. With reference to the previous reports, our SAC-1 electrode of high specific capacitance may be attributed to the combined effect of a high N and P doping level and a large BET surface area, which changes the electron donor/acceptor characteristics of carbon and increases the surface area accessibility for electrolyte ion transport. We take that as a proof of principle for the importance of structurally incorporated N and P for the enhancement of the supercapacitive performance. An ideal EDLC with an infinitely fast ion transport should deliver the same energy even ata high current rate. The relationships between capacitance and charge/discharge current density of SC and SAC electrodes are presented inFig.5c. The porous structure and suitable size distribution of meso/micropores of SAC grant efficient electrolytes transfer and electron transport at a high speed.[47] The SAC-1 electrode shows a specific capacitance of 275 F g^{-}

[1]even at a high current density of 20 A g^{-1} (~81 % retention compared with that of 0.5 A g^{-1}). It is reflected that the electrode material possesses agood capacitance retention capability and the capacitance is not kinetically limited.[48]

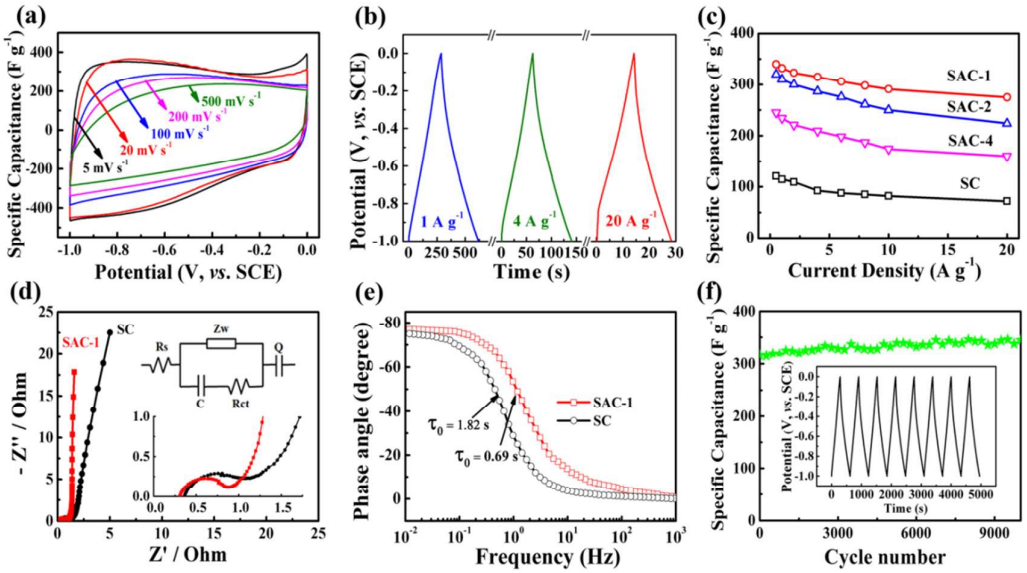

Fig. 5 (a) CV curves at different scan rates and (b) charge-discharge curves at different current densities of SAC-1 electrode. (c) Specific capacitances of SC and SAC electrodes at different current densities. (d) Nyquist plots and (e) bode plots of phase angle versus frequency of SC and SAC-1 electrodes. The inset in (d) show the high-frequency range and electrical equivalent circuit. (f) long-term cycling performances of SAC-1 electrode at 1 A g^{-1}.

The fast electrolyte transfer in the SC and SAC samples can be confirmed by the Nyquist plots (Fig.5d) recorded from 0.01 to 10 000 Hz at open-circuit voltage in 6M KOH. In the low-frequency region, SAC-1 has a steepcapacitive spike with an almost 90°angle relative to other samples, indicating good capacitive behavior (vertical line for an ideal capacitor). Thecorresponding value of the intercept on the X axis at high frequency (close to 100 kHz)represents the intrinsic ohmic resistance or ESR of the electrode material and electrolyte.The fittingof impedance data to the equivalent circuit model by the coupled nonlinear Schrçdinger equation method is also shown.[48, 49] Obviously, SAC-1 shows lower ESR value because the advantages of certain amount of heteroatom doping and a shortened path forion transport. The dependences of phase angle on the frequency for the SC and SAC-1 show that the phase angles of both devices areclose to -90°at low frequencies, confirming an ideal capacitivebehavior (Fig. 5e). The characteristic frequency at a phaseangle of -45°marks the point where the resistive and capacitiveimpedances are equal. The SC and SAC-1 exhibit an $f_0$of 0.55 Hz and 1.45 Hz, respectively, which corresponds to a timeconstantτ_0(=1/f_0) of 0.69 s for SAC-1, greatly lower than thatof SC (1.82 s). This rapid frequencyresponse of SAC-1 further suggests the significantly enhancedion transport rate within the electrodes.

In addition, the performance of SAC-1electrode is very stable. As shown in Fig.5f, during the initial 2, 000 galvanostatic charge/discharge cycles, SAC-1 showed slight capacitance increase, indicating the continuous penetration of electrolyte into carbon porous network. Then the capacitance was stable at320 Fg^{-1}after 10, 000cycles. It has been proven that the cycle performance of SAC-1 is even significantly better than other doped porous carbons. In addition to the advantageous porous structure, this may be related to the chemical inhibition of unstable oxygensurface species by N and P functional groups. The development of groups relative to the deterioration of capacitorsare suppressed and the cycle stability is improved.[42]

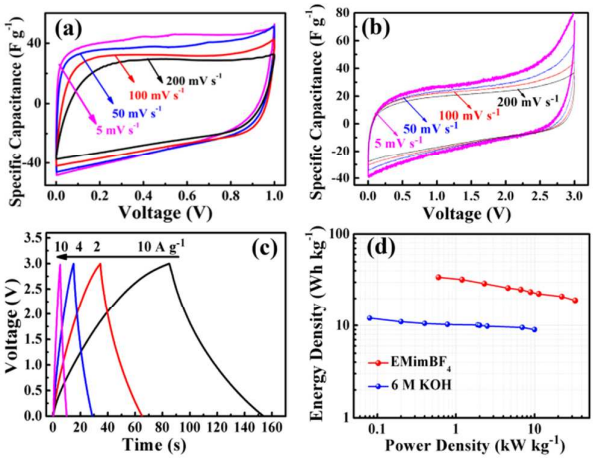

Fig.6 Electrochemical capacitive behaviour of SAC-1 measured in two-electrode systems: (a, b) CV curves at various scan rates in 6 M KOH and $EMImBF_4$ electrolyte, respectively; (c) galvanostatic charge–discharge curves at different current densities in $EMImBF_4$ electrolyte. (d) Ragone plots in 6 M KOH and $EMImBF_4$ electrolyte.

To completely determine the electrochemical capacitance and simulate the actual device behavior of SAC samples, further measurements of SAC-1 were conducted in a two-electrode system by both aqueous and ionic liquid electrolytes.

SAC-1 shows rectangular shaped CV curves between 0 and 1.0 V in 6 M KOH solution, which is the characteristic of ideal EDL capacitor with little electrolyte diffusion limitation (Fig. 6a). Incontrast to the three-electrode system, no apparent redox peaks are observed despite the presence of numerous heteroatoms in SAC-1, which is consistent with previous reports.[27, 50, 51] Moreover, in $EMImBF_4$,rectangular CV curves are attained from 0 to 3.0 V in Fig. 6b, showing characteristic of ideal EDL capacitors. In both electrolytes, the rectangular shapes can be maintained without drastic change at a high scan rate of 200 mV s^{-1}, which is attributed to the unique hierarchical porous nanostructure that favors fast ionic motion. The capacitance of SAC-1 in 6 M KOH is 312, 325, 306 and273 F g^{-1}at a current density of 1, 2, 4 and 20 A g^{-1}, respectively. In $EMImBF_4$, SAC-1 gives a specific capacitance up to 120 F g^{-1} at a low current density of 0.5A g^{-1}. A capacitance as high as 78 F g^{-1}can still be retainedeven at a high current density of 10 A g^{-1}. Further characterization of energy and power densities was demonstrated in ragon plots (Fig.7d). The plotclearly shows that the SAC-1 supercapacitor shows an energy density of 11.8Wh kg^{-1} at a relatively low power density of 85 $Wkg^{-1}$and still maintains 9.3Wh kg^{-1}at a high power density of 10.3 $kWkg^{-1}$ in KOH. Most importantly, in $EMImBF_4$, a high power density about $19Wkg^{-1}$is delivered with a very high energy density of 33.1Wh kg^{-1}. According to the above electrochemical results, our supercapacitors exhibit significantly higher energy and power densities compared to most previously reported symmetrical devices made of carbon nanotube, graphene and other porous carbon materials.Thus, the highly improved electrochemical performance of SAC is ascribed to its unique characteristics:1) the porous structure witha high surface area and high mesoporosity favors fast ion and charge transfer by providing short and continuous pathways; 2) good conductivity facilitates electrons transport, which is important for achieving high-rate performance and electrochemical stability; 3) remarkably, the presence of N and P species in SAC enhances its electrical conductivity and wettability, provides additional pseudocapacitance, and improves the cycle stability.

4. Conclusions

We have demonstrated that a common daily waste, fish scale, can be converted into a high-performance electrode material for supercapacitor. The special lamellar structure and inherent organic compositionof fish scale allowus to produceporous carbons with high SSA, high level of mesoporosity and abundant P and N functional groups. Because ofthese unique characterization, the SAC-1 sample displays excellent supercapacitive character (high specific capacitances of 340 F g^{-1} and 120 F g^{-1} in 6 M KOH and $EMImBF_4$ electrolyte, respectively; long stability over 10 000 cycles). Moreover, compared to conventional activated carbons used in commercial devices, the proposed scale-derived carbon offers leap forward in energy and power density improvement of supercapacitors.

Acknowledgements

This work was supported by the National Basic Research Program of China (973 Program) (No. 2014CB239701), National Natural Science Foundation of China (No. 21173120, 51372116), Natural Science Foundation of Jiangsu Province (BK2011030, BK20151468), the Fundamental Research Funds for the Central Universities of NUAA (NP2014403) and the Priority Academic Program Development of Jiangsu Higher Education Institutions (PAPD).

Notes and references

1. P. Simon and Y. Gogotsi, *Nature Materials*, 2008, **7**, 845-854.
2. E. Frackowiak and F. Beguin, *Carbon*, 2001, **39**, 937-950.
3. A. G. Pandolfo and A. F. Hollenkamp, *Journal of Power Sources*, 2006, **157**, 11-27.
4. L. L. Zhang and X. S. Zhao, *Chem. Soc. Rev.*, 2009, **38**, 2520-2531.
5. D.W. Wang, F. Li, M. Liu, G. Q. Lu and H.M. Cheng, *Angewandte Chemie-International Edition*, 2008, **47**, 373-376.
6. T. Tao, L. Zhang, H. Jiang and C. Li, *New Journal of Chemistry*, 2013, **37**, 1294-1297.
7. G. Wang, L. Zhang and J. Zhang, *Chem. Soc. Rev.*, 2012, **41**, 797-828.
8. C. Ramirez-Castro, O. Crosnier, L. Athouel, R. Retoux, D. Belanger and T. Brousse, *J. Electrochem. Soc.*, 2015, **162**, A5179-A5184.
9. X. Xu, J. Zhou, D. Nagaraju, L. Jiang, V. R. Marinov, G. Lubineau, H. N. Alshareef and M. Oh, *Adv. Funct. Mater*, 2015.
10. H. M. Jeong, J. W. Lee, W. H. Shin, Y. J. Choi, H. J. Shin, J. K. Kang and J. W. Choi, *Nano Lett.*, 2011, **11**, 2472-2477.
11. D.W. Wang, F. Li, L.C. Yin, X. Lu, Z.G. Chen, I. R. Gentle, G. Q. Lu and H.M. Cheng, *Chem. Eur. J.*, 2012, **18**, 5345-5351.
12. Z. Wen, X. Wang, S. Mao, Z. Bo, H. Kim, S. Cui, G. Lu, X. Feng and J. Chen, *Adv. Mater.*, 2012, **24**, 5610-5616.
13. L. Zhao, L.Z. Fan, M.Q. Zhou, H. Guan, S. Qiao, M. Antonietti and M.M. Titirici, *Adv. Mater.*, 2010, **22**, 5202-5206.
14. S. Yang, L. Zhi, K. Tang, X. Feng, J. Maier and K. Muellen, *Adv. Funct. Mater*, 2012, **22**, 3634-3640.
15. J. Han, L. L. Zhang, S. Lee, J. Oh, K.S. Lee, J. R. Potts, J. Ji, X. Zhao, R. S. Ruoff and S. Park, *ACS Nano*, 2013, **7**, 19-26.
16. L. Sun, Y. Fu, C. Tian, Y. Yang, L. Wang, J. Yin, J. Ma, R. Wang and H. Fu, *Chemsuschem*, 2014, **7**, 1637-1646.
17. D.W. Wang, F. Li, Z.G. Chen, G. Q. Lu and H.M. Cheng, *Chemistry of Materials*, 2008, **20**, 7195-7200.
18. D. Hulicova-Jurcakova, A. M. Puziy, O. I. Poddubnaya, F. Suárez-García, J. M. Tascón and G. Q. Lu, *J. Am. Chem. Soc.*, 2009, **131**, 5026-5027.
19. K. Singh, M. Seredych, E. Rodriguez Castellon and T. J. Bandosz, *ChemElectroChem*, 2014, **1**, 565-572.
20. C. H. Choi, S. H. Park and S. I. Woo, *J. Mater. Chem.*, 2012, **22**, 12107-12115.
21. L. Wei, M. Sevilla, A. B. Fuertes, R. Mokaya and G. Yushin, *Adv. Funct. Mater*, 2012, **22**, 827-834.

22. L. Qie, W. Chen, H. Xu, X. Xiong, Y. Jiang, F. Zou, X. Hu, Y. Xin, Z. Zhang and Y. Huang, *Energy Environ. Sci.*, 2013, **6**, 2497-2504.
23. C. Wu, X. Wang, B. Ju, L. Jiang, H. Wu, Q. Zhao and L. Yi, *J. Power Sources*, 2013, **227**, 1-7.
24. J. W. To, Z. Chen, H. Yao, J. He, K. Kim, H.H. Chou, L. Pan, J. Wilcox, Y. Cui and Z. Bao, *ACS Cent. Sci.*, 2015, **1**, 68-75.
25. E. Ra, E. Raymundo-Piñero, Y. Lee and F. Béguin, *Carbon*, 2009, **47**, 2984-2992.
26. S. Dutta, A. Bhaumik and K. C.W. Wu, *Energy Environ. Sci.*, 2014, **7**, 3574-3592.
27. Z. Li, Z. Xu, X. Tan, H. Wang, C. M. Holt, T. Stephenson, B. C. Olsen and D. Mitlin, *Energy Environ. Sci.*, 2013, **6**, 871-878.
28. J. Li and Q. Wu, *New Journal of Chemistry*, 2015, **39**, 3859-3864.
29. S. Gao, Y. Chen, H. Fan, X. Wei, C. Hu, H. Luo and L. Qu, *J. Mater. Chem. A*, 2014, **2**, 3317-3324.
30. S. Gao, L. Li, K. Geng, X. Wei and S. Zhang, *Nano Energy*, 2015, **16**, 408-418.
31. Y. S. Yun, S. Y. Cho, J. Shim, B. H. Kim, S. J. Chang, S. J. Baek, Y. S. Huh, Y. Tak, Y. W. Park and S. Park, *Adv. Mater.*, 2013, **25**, 1993-1998.
32. Z. Li, L. Zhang, B. S. Amirkhiz, X. Tan, Z. Xu, H. Wang, B. C. Olsen, C. Holt and D. Mitlin, *Adv. Energy Mater.*, 2012, **2**, 431-437.
33. E. Raymundo‐Piñero, F. Leroux and F. Béguin, *Adv. Mater.*, 2006, **18**, 1877-1882.
34. W. Qian, F. Sun, Y. Xu, L. Qiu, C. Liu, S. Wang and F. Yan, *Energy Environ. Sci.*, 2014, **7**, 379-386.
35. X.L. Wu, T. Wen, H.L. Guo, S. Yang, X. Wang and A.W. Xu, *ACS nano*, 2013, **7**, 3589-3597.
36. L. Wang, G. Mu, C. Tian, L. Sun, W. Zhou, P. Yu, J. Yin and H. Fu, *Chemsuschem*, 2013, **6**, 880-889.
37. T. Ikoma, H. Kobayashi, J. Tanaka, D. Walsh and S. Mann, *Journal of Structural Biology*, 2003, **142**, 327-333.
38. S. Zhao, C. Li, W. Wang, H. Zhang, M. Gao, X. Xiong, A. Wang, K. Yuan, Y. Huang and F. Wang, *Journal of Materials Chemistry A*, 2013, **1**, 3334-3339.
39. C. Wang, Y. Zhou, L. Sun, Q. Zhao, X. Zhang, P. Wan and J. Qiu, *The Journal of Physical Chemistry C*, 2013, **117**, 14912-14919.
40. V. Barranco, M. Lillo-Rodenas, A. Linares-Solano, A. Oya, F. Pico, J. Ibañez, F. Agullo-Rueda, J. Amarilla and J. Rojo, *The Journal of Physical Chemistry C*, 2010, **114**, 10302-10307.
41. Y.H. Lee, K.H. Chang and C.C. Hu, *J. Power Sources*, 2013, **227**, 300-308.
42. T. Kim, G. Jung, S. Yoo, K. S. Suh and R. S. Ruoff, *ACS Nano*, 2013, **7**, 6899-6905.
43. C. O. Ania, V. Khomenko, E. Raymundo‐Piñero, J. B. Parra and F. Beguin, *Adv. Funct. Mater*, 2007, **17**.
44. L.F. Chen, X.D. Zhang, H.W. Liang, M. Kong, Q.F. Guan, P. Chen, Z.Y. Wu and S.H. Yu, *ACS Nano*, 2012, **6**, 7092-7102.
45. T. Kim, G. Jung, S. Yoo, K. S. Suh and R. S. Ruoff, *ACS Nano*, 2013, **7**, 6899-6905.
46. L. Wang, L. Sun, C. Tian, T. Tan, G. Mu, H. Zhang and H. Fu, *RSC Adv.*, 2012, **2**, 8359-8367.
47. L. Wang, G. Mu, C. Tian, L. Sun, W. Zhou, T. Tan and H. Fu, *ChemSusChem*, 2012, **5**, 2442-2450.
48. L. Yang, S. Cheng, Y. Ding, X. Zhu, Z. L. Wang and M. Liu, *Nano Lett.*, 2011, **12**, 321-325.
49. C. Guo, N. Li, L. Ji, Y. Li, X. Yang, Y. Lu and Y. Tu, *J. Power Sources*, 2014, **247**, 660-666.
50. M. D. Stoller and R. S. Ruoff, *Energy Environ. Sci.*, 2010, **3**, 1294-1301.
51. Z. Wen, X. Wang, S. Mao, Z. Bo, H. Kim, S. Cui, G. Lu, X. Feng and J. Chen, *Adv. Mater.*, 2012, **24**, 5610-5616.

TOC

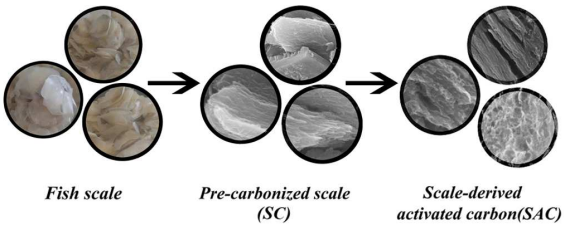

Fish scale-derived carbon, prepared through chemical activation, exhibits excellent supercapacitive performance in aqueous and ionic liquid electrolyte.